Available online at www.sciencedirect.com

ScienceDirect

Ceramics International 40 (2014) 163–172

CERAMICS INTERNATIONAL

www.elsevier.com/locate/ceramint

Strengthening mechanism of graphene oxide nanosheets for Al_2O_3–C refractories

Qinghu Wang, Yawei Li*, Ming Luo, Shaobai Sang, Tianbin Zhu, Lei Zhao

The Hubei Province Key Laboratory of Ceramics and Refractories, Wuhan University of Science & Technology, Wuhan 430081, PR China

Received 24 February 2013; received in revised form 29 May 2013; accepted 29 May 2013
Available online 5 June 2013

Abstract

Al_2O_3–C refractories containing graphene oxide nanosheets (GONs) and additives of Al, Si and SiO_2 were prepared. The GONs/α-Al_2O_3 composite powders were prepared by ball milling expanded graphite (EG) with micron sized α-Al_2O_3, and then used to make the Al_2O_3–C refractory specimens. The results showed that GONs were distributed well in α-Al_2O_3 powder by ball milling, and the size and thickness of GONs depended on the amount of expanded graphite added. The GONs enhanced the formation of ceramic whiskers in the specimens at lower temperature owing to their higher reactivity than graphite flake. The mechanical properties such as cold modulus of rupture (CMOR), flexural modulus (E), force and displacement curves of Al_2O_3–C refractories with GONs were improved compared with those without GONs. This improvement was attributed to the strengthening effects of GONs at 800 °C and the synergetic strengthening effects with graphite flake and the in-situ formed whiskers at 1000–1400 °C.

Keywords: Graphene oxide nanosheets; Microstructure; Strengthening; Al_2O_3–C refractories

1. Introduction

Carbon containing refractories have been widely used in steelmaking industries owing to their excellent corrosion resistance and thermal shock resistance [1–5]. However, with the development of low carbon and ultra low carbon steelmaking technology, traditional carbon containing refractories which have relatively high carbon content (12–18 wt%) cannot meet the requirements because of carbon pick-up in molten steel. Therefore, it's imperative to develop low carbon containing refractories (5 wt% C, or even lower than 3 wt% C) with high performance. Generally, graphite flake is the typical carbon source for traditional carbon containing refractories. However, the mechanical properties of carbon containing refractories normally deteriorate by simply decreasing the carbon amount.

Recently, nanosized carbon sources have been introduced as carbon source into carbon containing refractories to produce nanostructural matrix for high performance [6,7]. On the one hand, they fill more easily not only in the tiny spaces between the coarse, medium and fine particles in the specimen but also in the interior pores and gaps, which contribute to reduce the porosity, increase the densification, strength and corrosion resistance [8]. On the other hand, these kinds of nanosized carbon with different morphologies can absorb and relieve the thermal stress, and thereby improve the thermal shock resistance. Carbon black as zero-dimension nanosized carbon source has been widely used in MgO–C refractories. Mousom Bag [9] found that the thermal shock resistance of MgO–C refractory was improved with the addition of nano carbon black. Nano-tech magnesia carbon bricks showed outstanding properties such as thermal shock resistance, corrosion resistance, oxidation resistance using nano-sized hybrid graphite black [10,11]. Moreover, carbon nanotubes (CNTs) as one dimensional carbon source have attracted considerable attention in carbon containing refractories due to their excellent physical, chemical and mechanical properties [12,13]. Luo et al. [14] found that Al_2O_3–C refractories containing multi-walled carbon nanotubes (MWCNTs) possessed better mechanical properties, than that without addition of MWCNTs. Roungos et al. [15] reported that the addition of carbon nanotubes and alumina nanosheets into Al_2O_3–C

*Corresponding author. Tel.: +86 27 68862188; fax: +86 27 68862018.
E-mail addresses: liyawei@wust.edu.cn, liyaweiwust@hotmail.com (Y. Li).

0272-8842/$ - see front matter © 2013 Elsevier Ltd and Techna Group S.r.l. All rights reserved.
http://dx.doi.org/10.1016/j.ceramint.2013.05.117

refractories resulted in excellent thermal shock performance. What's more, owing to the high specific surface area and reactivity, these forms of nano-carbon can easily react with other additions to form the nano-sized ceramic phases which reinforce and toughen the refractories [16–19].

Recently another nanosized two-dimension carbon source, graphene nanosheets with nanoscale thickness and better mechanical properties compared with graphite flake, have been incorporated into ceramic or polymer materials to improve their mechanical properties [20–22]. Wang et al. [23] reported that the fracture toughness of the graphene nanosheet/alumina composite was about 53% orders of magnitude higher than that of unreinforced alumina material. Ramanathan et al. [22] found that polymers containing functionalized graphene sheets offered the mechanical properties equal to or even better than those containing single walled carbon nanotubes.

In the present work, GONs are incorporated to strengthen the Al_2O_3–C refractories. GONs themselves can improve the mechanical properties at lower temperature based on the two dimensional structures. Meanwhile, GONs can promote the formation of SiC whiskers in the Al_2O_3–C refractories at high temperatures. Fan [24] obtained larger displacement and greater force in graphite flake containing Al_2O_3–C refractories than carbon black containing refractories because of the much more curved SiC whiskers contributed by graphite flake. GONs have the same structure as graphite flake and higher reactivity than that of the latter, therefore it can strengthen Al_2O_3–C refractories with much more SiC whiskers.

2. Experimental

2.1. Preparation of GONs/α-Al_2O_3 composite powders

In the experiment, expanded graphite was firstly manufactured by exfoliating commercial expandable graphite (50 mesh, 98% C, Shangdong, China) in microwave oven for 20 s. Then certain amount of expanded graphite was mixed with α-Al_2O_3 (2 μm, 99% Al_2O_3, Kaifeng Special Refractories Co., Ltd., China) and wet milled with N-methyl-pyrrolidone (NMP) at room temperature for 7 h in a conventional planetary ball milling. The weight ratio of balls to powder was 1:1, and the rotation rate of the vial was 400 rpm. After ball milling, the composite powders were dried at 60 °C for 120 h. The ratios of α-Al_2O_3 to expanded graphite were 100:0, 100:1, 100:2.1, 100:5.5 and 100:8.8, and the mixtures were designated as N0, N10, N21, N55 and N88, respectively.

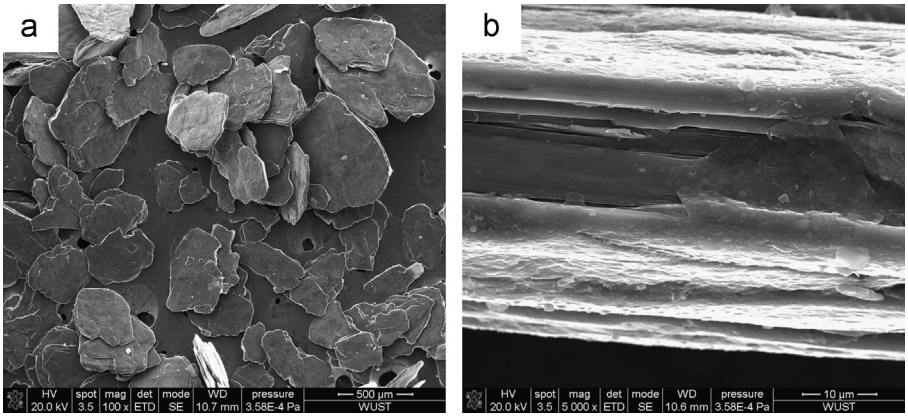

Fig. 1. Low (a) and high (b) magnification image of expandable graphite.

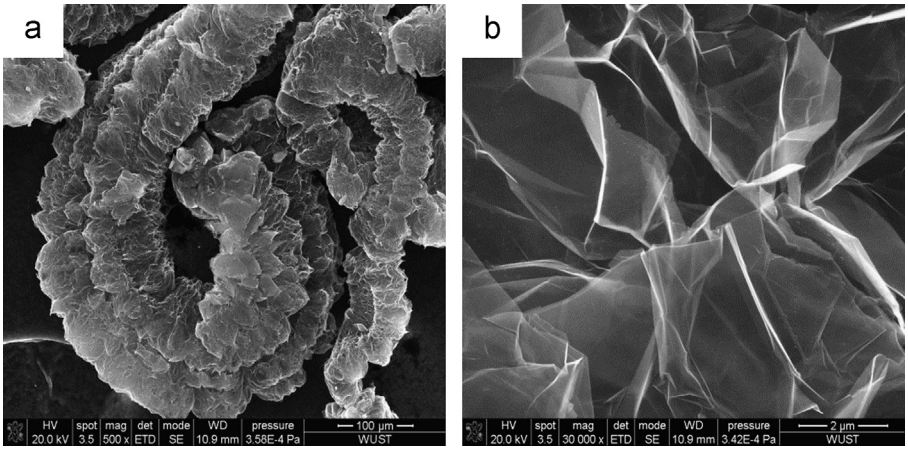

Fig. 2. Low (a) and high (b) magnification image of expanded graphite.

2.2. Preparation of Al_2O_3–C refractories specimens

Tabular alumina (8–14 mesh, 14–28 mesh, 28 mesh, 325 mesh and 20 μm, 99.5 wt% Al_2O_3, Qingdao Almatis Co., Ltd., China), aluminum powder (45 μm, 99 wt% Al), silicon powder (45 μm, 98.47 wt% Si, China), microsilica powder (0.5 μm, 97 wt% SiO_2, China), graphite flake (200 mesh, 97.58 wt% fixed carbon, China) were used as raw materials. In addition, thermosetting phenolic resin (liquid, > 40% fixed carbon, Wuhan Lifa Chemistry & Industry Co., Ltd., China) was added as binder. The basis batch composition (labeled as GN0) consisted of 83 wt% tabular alumina, 2 wt% Al powder, 3 wt% Si powder, 1 wt% microsilica powder, 1 wt% graphite flake and 10 wt% N0 powder. On the basis of GN0, different amount of as-milled powders such as 10.1 wt% N10, 10.21 wt% N21, 10.55 wt% N55 and 10.88 wt% N88, were incorporated into the material to replace N0 powder (labeled as GN10, GN21, GN55 and GN88, respectively), and the amount of graphite flake was adjusted to control the carbon

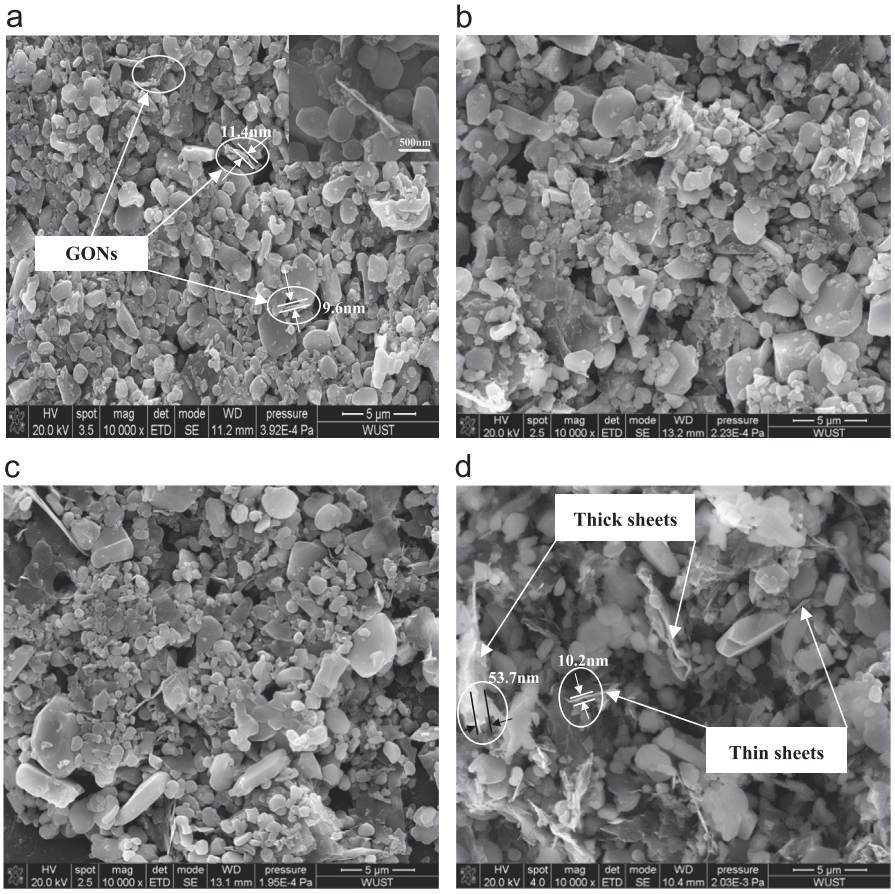

Fig. 3. SEM micrographs of the ball milled composite powders of (a) N10, (b) N21, (c) N55 and (d) N88.

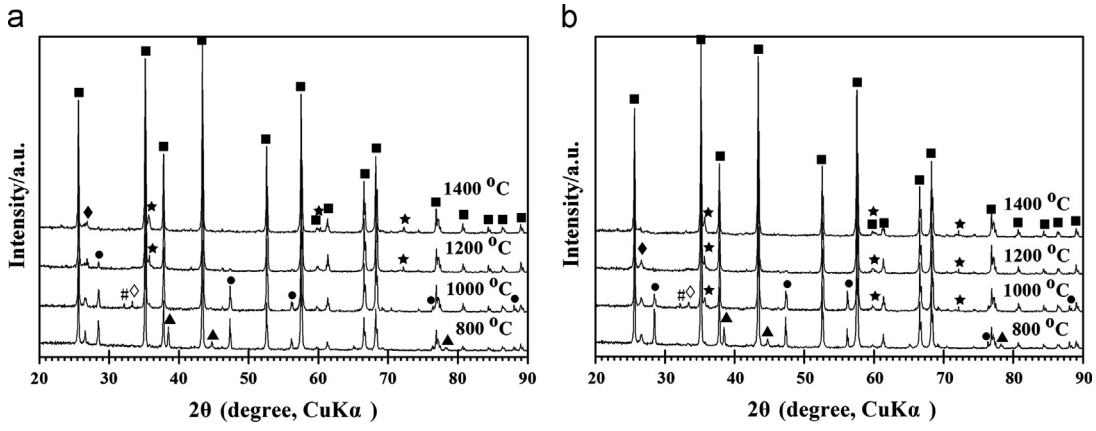

Fig. 4. XRD patterns of specimens GN0 and GN88 fired at different temperatures. (a) specimen GN0 and (b) specimen GN88. ■-Corundum, ★-β-SiC, ●-Si, #-Al_4C_3, ◇-AlN, ▲-Al, ◆-graphite.

content of 1 wt% in all the composite. All the raw materials were mixed for 30 min in the mixer with the rotation rate of 80–120 rpm. Then, specimens of 25 mm in width, 25 mm in height and 100 mm in length were fabricated by cold pressing at 150 MPa and cured at 160 °C for 24 h. After that, the as-prepared specimens were placed inside a corundum sagger which was filled with petroleum coke powder. Finally, the whole sagger was then placed into an electrical furnace and heated from room temperature to 800 °C, 1000 °C, 1200 °C and 1400 °C with a heating rate of 5 °C/min and a holding time of 3 h before cooling to room temperature.

2.3. Testing and characterization methods

Mechanical properties including cold modulus of rupture (CMOR) and modulus of elasticity (*E*) were measured by using the three-point bending test at ambient temperature with a span of 80 mm and a loading rate of 0.5 mm/min by means of electronic digital control system (EDC 120, DOLI Company, Germany). The force–displacement curve of each refractory specimen was recorded simultaneously during the test. All the preceding measurements were carried out with three samples for each composition. The microstructures of ruptured surfaces of all the fired Al_2O_3–C refractories were observed by a field emission scanning electron microscope (FESEM, Quanta 400, FEI Company, USA) equipped with energy dispersive X-ray spectroscope (EDS, Noran 623 M-3SUT, Thermo Electron Corporation, Japan). The phase compositions of the fired specimens were analyzed by X-ray diffraction (XRD, X' Pert Pro, Philips, Netherlands). Thermogravimetry-differential scanning calorimetry (TG-DSC, STA499, NETZSCH, Germeny) was employed to evaluate the reactivity and calculate non-isothermal oxidation kinetics of the graphite flake and expanded graphite (EG).

3. Results and discussion

3.1. Microstructures of expanded graphite and its ball-milled composite powder

Fig. 1 shows the SEM micrographs of the expandable graphite particles. The expandable graphite flake is irregular in shape (Fig. 1a). Magnified image reveals that the individual expandable graphite particle is approximately 300 μm in length and 35 μm in thickness (Fig. 1b). Expanded graphite (EG) manufactured by exfoliating expandable graphite in microwave oven, has a loose, worm-like structure and a large amount of pores (Fig. 2a), with the length of about 900 μm and layer thickness of about 10 nm (Fig. 2b), similar to other reports [25,26].

As shown in Fig. 3, the ball milled composite powders containing different ratios of GONs to α-Al_2O_3 have been fabricated by ball milling EG with α-Al_2O_3. For sample N10, GONs with length of 2–3 μm and thickness of approximately

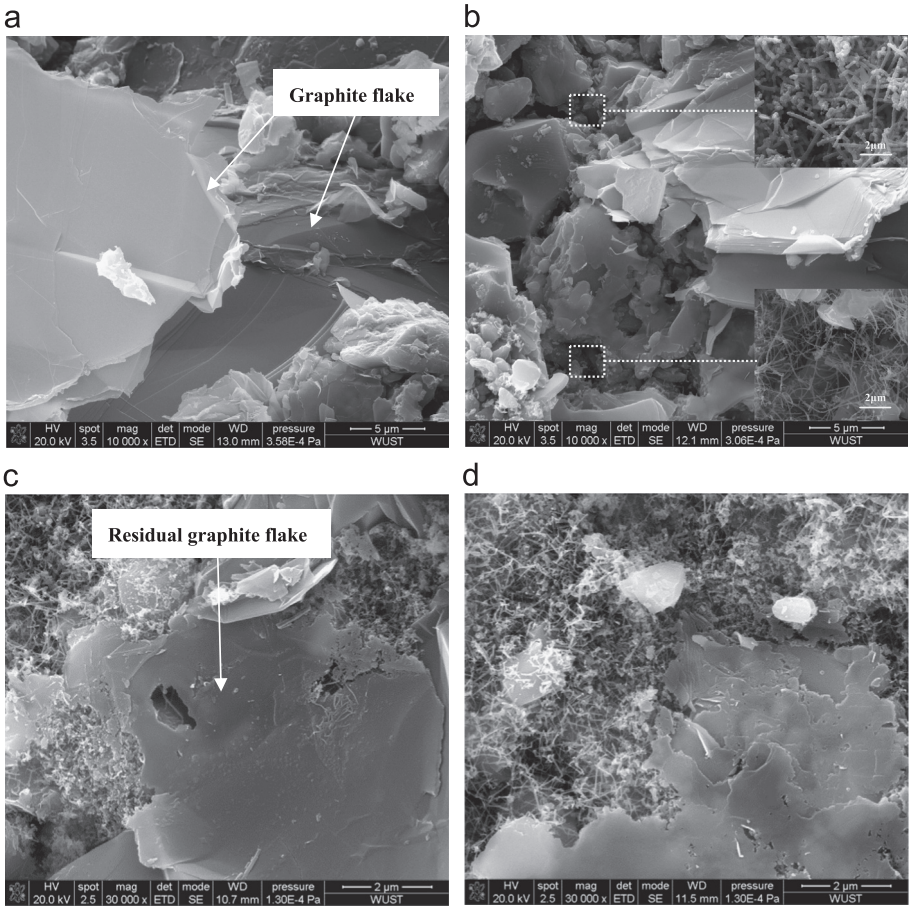

Fig. 5. SEM micrographs of specimen GN0 fired at different temperatures. (a) 800 °C, (b) 1000 °C, (c) 1200 °C and (d) 1400 °C.

10 nm are embedded into α-Al_2O_3 (Fig. 3a). With the addition of expanded graphite, the amount and size of GONs increased remarkably (Fig. 3b–d). Moreover, compared with N10, it can be observed clearly that not only thin sheets (10 nm), but also large amount of thick sheets (50 nm) appeared in the N88 powder in Fig. 3d. However, Fan et al. [27] reported that most of the pulled-out sheets were 50 nm in thickness and no thin GONs (below 20 nm) was observed, which was explained that too thin sheets cannot be identified by a SEM image. The thin sheets were also easy to rupture under the shearing stress, yet the thick sheets are strong enough to withstand the shearing shear stress. In other words, the ball milling of α-Al_2O_3 and different amounts of EG could fabricate different composite powders with various GONs amount, size and thickness.

3.2. Phase composition

In order to understand the effect of GONs on the phase evolution of Al_2O_3–C refractories fired in the temperature range from 800 to 1400 °C, all the specimens are examined by X-ray diffraction (Fig. 4). For the specimen GN0 fired at 800 °C, only corundum, graphite, Al, Si phases were detected, demonstrating that no new phase formed at this temperature. At 1000 °C, the Al phase disappeared, but AlN and Al_4C_3 phases formed in the specimens. At 1200 °C, the AlN and Al_4C_3 phases disappeared, but the SiC phase was detected in the specimens instead. Up to 1400 °C, the Si phase disappeared whereas the peak intensity of SiC phase increased a little (Fig. 4a). With regard to the specimens containing GONs, it seems that the GONs had an influence on the phase forming or disappearing temperature compared with specimen without GONs. For example, in the specimen GN88, the SiC phase formed at 1000 °C, while the Si and graphite phases disappeared at 1200 °C and 1400 °C, respectively (Fig. 4b). These differences in phase composition of specimens may be closely associated to the reactivity of GONs and graphite flake.

3.3. Microstructure

The SEM micrographs of ruptured surfaces of all the specimens are shown in Figs. 5–7. In the specimens without GONs, it can be seen that the graphite flake remained intact and no ceramic phases were presented in the specimen fired at 800 °C (Fig. 5a). At 1000 °C, a few striated or curved whiskers were observed in alumina-riched region (Fig. 5b), which were confirmed to be AlN or Al_4C_3 whiskers according to the XRD and EDS analysis. When the specimens were fired at 1200 °C, many SiC whiskers grew from the particle boundaries of partially disintegrated graphite flake (Fig. 5c), which were in agreement with our previous observations [24]. At 1400 °C, the amount of SiC whiskers increased continually (Fig. 5d).

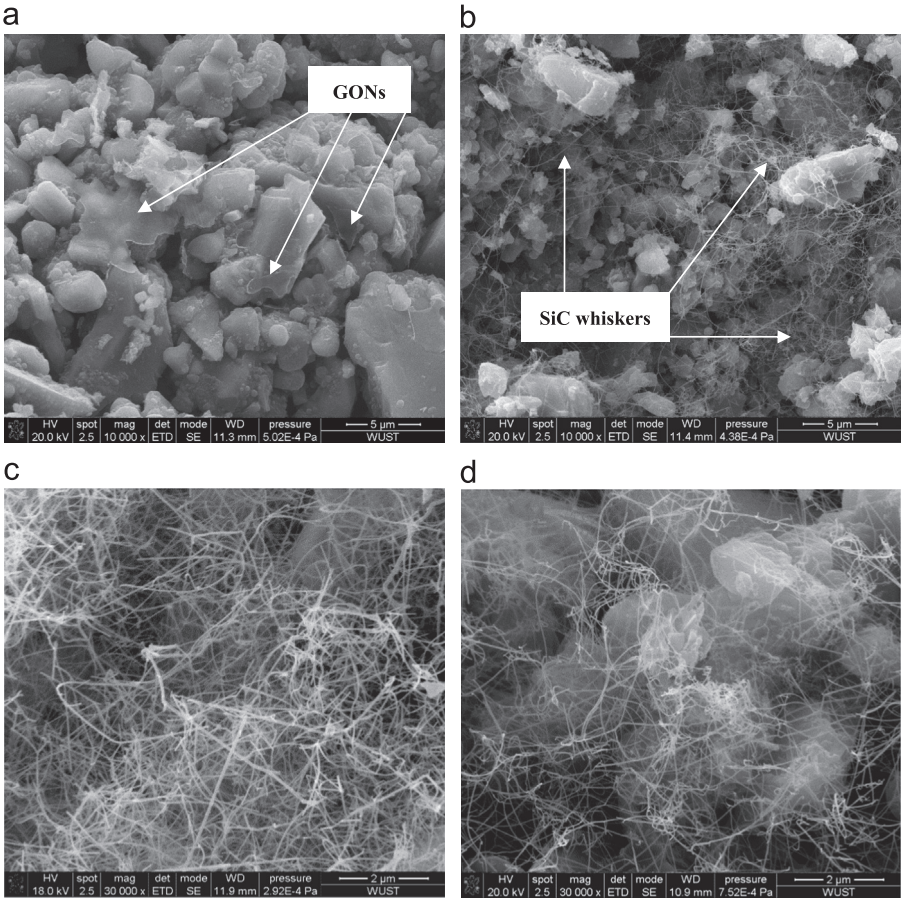

Fig. 6. SEM micrographs of specimen GN21 fired at different temperatures. (a) 800 °C, (b) 1000 °C, (c) 1200 °C and (d) 1400 °C.

With regard to the specimens containing GONs, it can be found that GONs were homogeneously dispersed in the matrix of specimens, for example, in GN21 (Fig. 6a). In contrast, when increasing the temperature to 1000 °C, besides the formation of some AlN or Al_4C_3 whiskers, large amount of SiC whiskers with high aspect ratio turned out in the specimen surprisingly (Fig. 6b). Up to 1200 °C, the amount of SiC whiskers increased continually (Fig. 6c). At 1400 °C, large amount of SiC whiskers formed, which interlocked with each other to form the intertextures and distributed well in the matrix. However, the aspect ratio decreased in comparison with the specimen fired at 1200 °C (Fig. 6d). With the addition of GONs, much more GONs dispersed homogeneously in the matrix, for example, in the specimen GN88 at 800 °C (Fig. 7a). More SiC whiskers formed and located in the matrix at 1000 °C (Fig. 7b) compared with GN21. At 1200 °C, the amount of SiC whiskers increased continually and they interlocked together with each other (Fig. 7c). With further increase in firing temperature to 1400 °C, the amount of SiC whiskers decreased slightly (Fig. 7d), and the length became shorter compared to the specimens fired at 1200 °C.

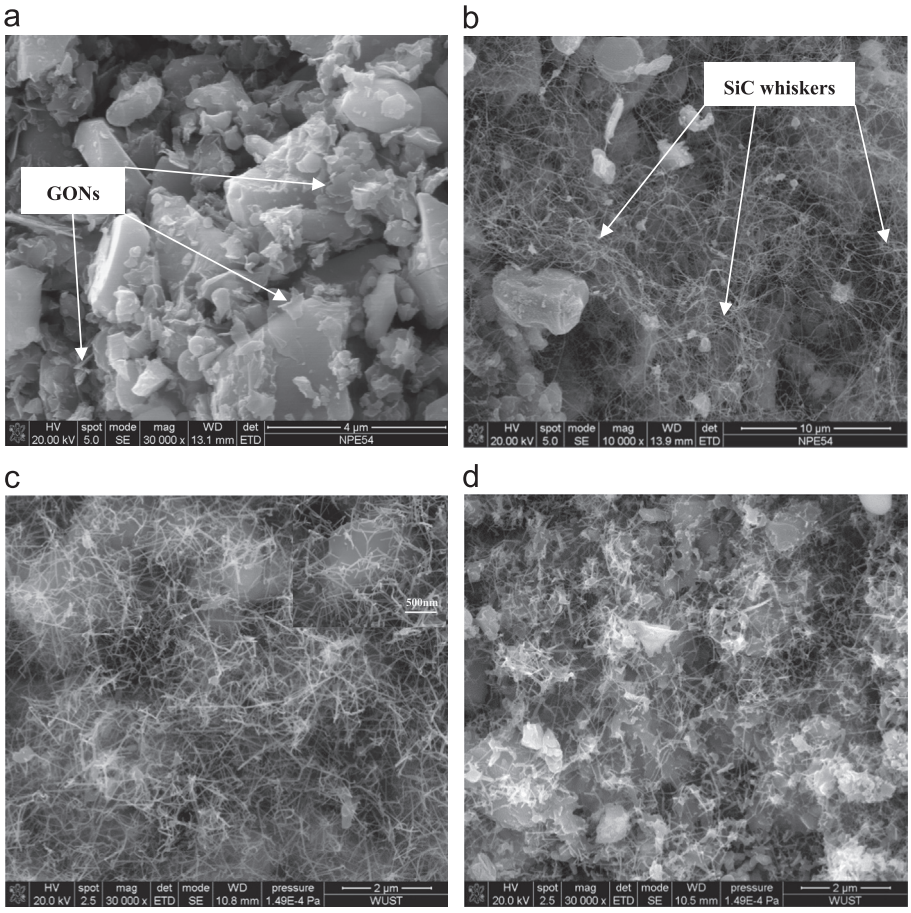

Fig. 7. SEM micrographs of specimen GN88 fired at different temperatures. (a) 800 °C, (b) 1000 °C, (c) 1200 °C and (d) 1400 °C.

Table 1
CMOR and *E* of specimens with different amounts of GONs fired at various temperatures.

Temperature	Index	GN0	GN10	GN21	GN55	GN88
800 °C	CMOR (MPa)	6.61 ± 0.29	9.64 ± 0.01	10.15 ± 0.16	10.37 ± 0.01	9.33 ± 0.19
	E (GPa)	1.64 ± 0.01	2.29 ± 0.01	2.09 ± 0.01	2.19 ± 0.07	1.77 ± 0.04
1000 °C	CMOR (MPa)	7.30 ± 0.11	12.22 ± 0.13	12.88 ± 0.06	11.41 ± 0.13	11.29 ± 0.03
	E (GPa)	1.63 ± 0.04	2.41 ± 0.07	2.50 ± 0.10	2.49 ± 0.08	2.16 ± 0.07
1200 °C	CMOR (MPa)	17.16 ± 0.23	23.25 ± 0.28	25.60 ± 0.08	23.29 ± 0.17	19.51 ± 0.28
	E (GPa)	2.87 ± 0.03	3.32 ± 0.06	3.48 ± 0.02	3.45 ± 0.03	3.11 ± 0.06
1400 °C	CMOR (MPa)	15.39 ± 0.35	17.21 ± 0.11	21.31 ± 0.28	15.43 ± 0.37	15.41 ± 0.28
	E (GPa)	2.94 ± 0.08	3.19 ± 0.03	3.10 ± 0.06	3.10 ± 0.08	2.83 ± 0.06

3.4. Mechanical properties

Mechanical properties including CMOR and E of Al_2O_3–C refractories were measured using the three-point bending test at room temperature, and the results are presented in Table 1. The values of CMOR and *E* of the specimens increased simultaneously with the firing temperature from 800 to 1200 °C, and then decreased suddenly at 1400 °C. For specimen GN0, the CMOR and *E* values at 800 °C were 6.61 MPa and 1.64 GPa, respectively. Then, they increased persistently to the maximum values of 17.16 MPa and 2.87 GPa at 1200 °C, yet decreased to 15.39 MPa and 2.94 GPa, respectively. It's notable that the specimens containing 0.21 wt% GONs presented larger CMOR and *E* values when the firing temperature ranging from 1000 °C to 1400 °C. Nevertheless, the CMOR and E for specimens fired at the same temperature values decreased with the addition of GONs.

The force–displacement curves of Al_2O_3–C refractories fired at 800 °C, 1000 °C, 1200 °C and 1400 °C were shown in Fig. 8. It can be seen that the force and displacement values of the specimens fired at different temperatures displayed the same trend as the values of CMOR and *E*. That's to say, the force and displacement values of the specimens increased continually with the increasing temperature from 800 to 1200 °C, but decreased at 1400 °C. Meanwhile, the specimens containing GONs demonstrated greater force and larger displacement, no matter what firing temperature was. Moreover, the specimens containing 0.88 wt% GONs showed larger displacement for the coking temperature ranging from 800 to 1000 °C. However, with the increase of firing temperature up to 1200 °C and 1400 °C, the specimens containing 0.21 wt% GONs presented greater force and larger displacement values.

3.5. Discussion

Based on the results presented above, the mechanical properties of Al_2O_3–C refractories were strongly dependent on the microstructural evolution in the temperature range from 800 to 1400 °C. In our experiment, tabular corundum,

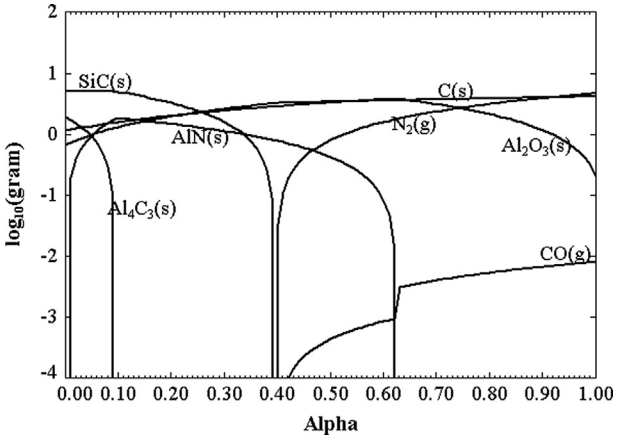

Fig. 9. Phase changes of Al_2O_3–C refractories at 1000 °C.

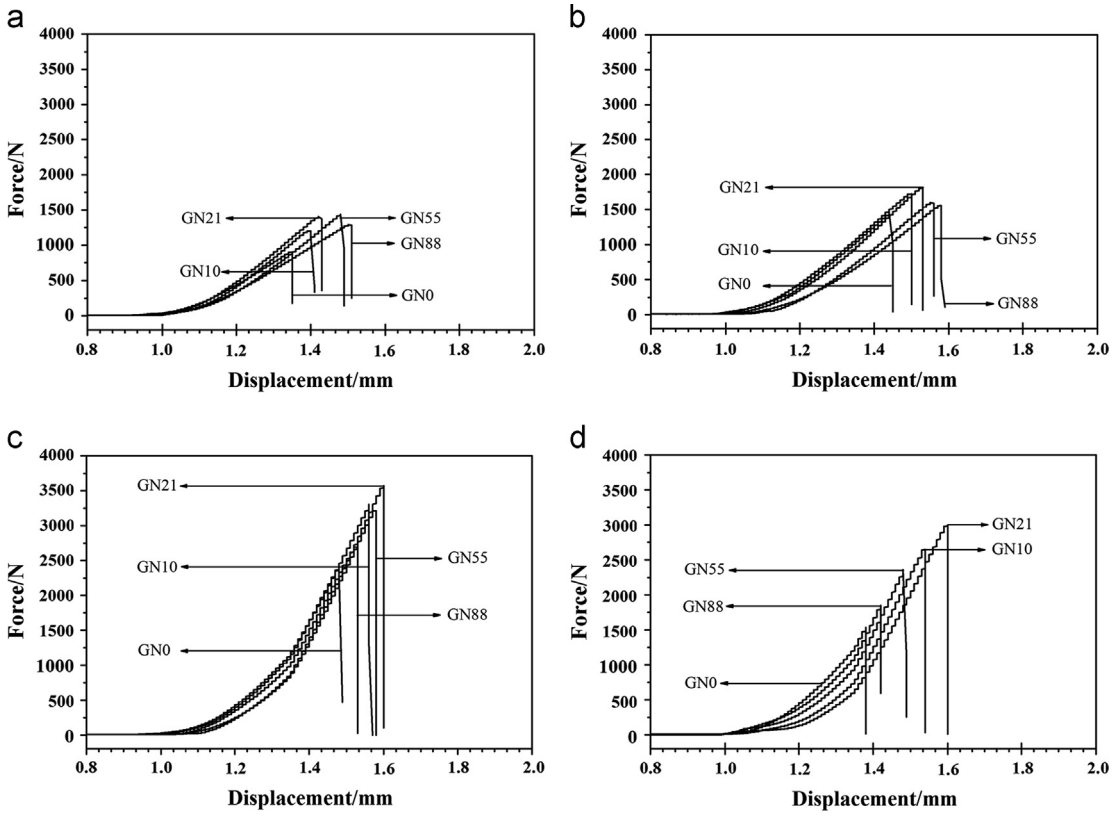

Fig. 8. Force—displacement curves of the specimens fired at different temperatures. (a) 800 °C, (b) 1000 °C, (c) 1200 °C and (d) 1400 °C.

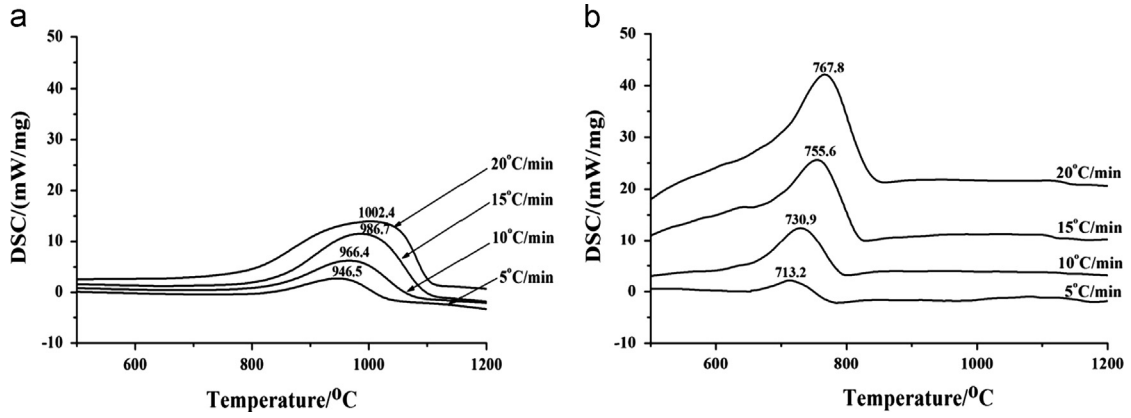

Fig. 10. Heating rate dependence of DSC curves for the oxidation of (a) graphite flake, and (b) expanded graphite.

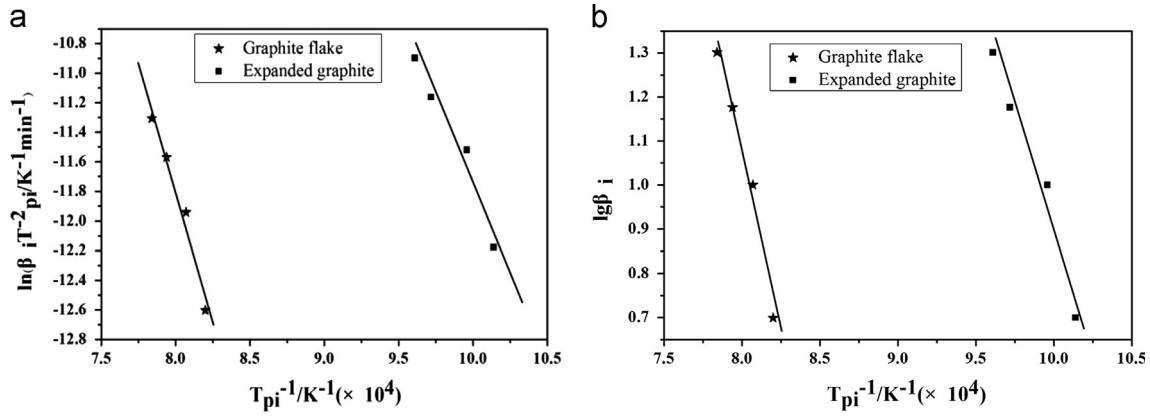

Fig. 11. Kissinger plots, $\ln(\beta_i/T_{pi}^2)$ vs. $1/T_{pi}$ (a); Ozawa plots, $\ln\beta_i$ vs. $1/T_{pi}$ (b).

metal aluminum, silicon, reactive alumina, microsilica, GONs and graphite are used as raw materials to prepare the Al_2O_3–C refractories in coke bed. The possible new phases to form in the matrix of refractories at high temperature can be predicted via thermodynamic calculation.

Equilibrium thermodynamic calculations were performed using the FACT package together with Gibbs energy minimization module EQUILIBRIUM. The atmosphere in the petroleum coke bed to fire all the specimens is approximately 0.35 atm CO and 0.65 atm N_2 [28]. Assuming the corundum and reactive alumina are not involved in the reactions in this system, Al_2O_3 was not included in the calculations. Therefore, 2 g Al, 3 g Si, 1 g SiO_2 and 2.6 g C (including 1 g C from graphite and 1.6 g fixed carbon from liquid resin), which were the composition of the matrix in Al_2O_3–C refractories, were included as starting batch composition for the calculations. Alpha is the weight ratio of atmosphere to matrix mass [29]. The results were plotted as log gram number of phase species as a function of Alpha.

The relationship of all the phases at 1000 °C with Alpha value is shown in Fig. 9. The phase evolution in the system is closely related to the Alpha value. For instance, when Alpha is close to 0, the partial pressures of CO and N_2 are very low, and SiC and Al_4C_3 form simultaneously. With the increase of Alpha, the amount of Al_4C_3 and SiC decreases gradually, finally achieves their minimum value when Alpha reaches 0.09 and 0.39, respectively. Moreover, the amount of AlN begins to increase when Alpha increases from 0.01 to 0.10, and reaches the maximum when Alpha is 0.10. The amount of AlN begins to decrease steadily when Alpha increases from 0.10. All the new phases in Al_2O_3–C refractories at the elevated temperature are calculated by Factsage software and are in agreement with the results of XRD analyses.

Table 2
The oxidation activation energy (kJ/mol) of graphite flake and expanded graphite in air.

Methods	Graphite flake	Expanded graphite
Kissinger	293.53	202.58
Ozawa	291.27	208.24

Analyzing the XRD patterns, there is no obvious difference of new phase species in all specimens except for the phase forming or disappearing temperatures. For example, the SiC

phase formed in the specimen GN88 at 1000 °C (Fig. 7b) and in the specimen GN0 at 1200 °C (Fig. 5c); the Si phase disappeared in the specimens GN88 at 1200 °C (Fig. 7c), but it no longer existed only at 1400 °C in the specimens GN0 (Fig. 5d). Such difference is closely related to the difference in the reactivity of carbon sources. GONs possessed higher reactivity than graphite flake. The addition of GONs with higher reactivity into Al_2O_3–C refractories promoted the formation of SiC phase and the decrease of Si phase. Meanwhile, the amount and the aspect ratio of SiC whiskers were much larger in the specimens containing GONs at 1000 °C and 1200 °C, which resulted in better mechanical properties of specimens containing GONs. In contrast, the SiC whiskers were difficult to be found in the specimen GN0 fired at 1000 °C. With the increase of firing temperature to 1400 °C, the contribution of GONs to the mechanical properties transferred to that of graphite flake because graphite flake had been prevailed to produce SiC whiskers at high temperature. However, the combination of graphite flake and GONs as carbon source produced positive influence on the mechanical properties of Al_2O_3–C refractories.

With respect to the reactivity of carbon source, non-isothermal kinetics, both Kissinger and Ozawa methods, were employed to study the oxidation kinetics of GONs and graphite flake in our experiment. EG was represented for GONs because of their similar nature. Calorimetic signals of phase transformation were monitored in DSC analysis when the continuous-heating regime was used from room temperature to 1200 °C at a heating rate of 5–20 °C/min. Fig. 10 shows the heating rate dependence of DSC curves for EG and graphite flake (50 mesh, 98% C, Shangdong, China). It is obvious that the exothermic oxidation peak of EG was much sharper and the temperature was lower compared with graphite flake at the same heating rate. The Kissinger and Ozawa curves of EG and graphite flake are depicted in Fig. 11.

For the Kissinger method, the equation [30],

$$\ln\left(\frac{\beta_i}{T_{pi}^2}\right) = \ln\frac{A_k R}{E_k} - \frac{E_k}{R}\frac{1}{T_{pi}}$$

where β_i refers to the heating rate, T_{pi} is the peak temperature of the maximal mass loss rate. R is the gas constant, while the model parameters A_k and E_k are the frequency factor and activation energy, respectively. The Ozawa equation is based on the following equation [31]:

$$\lg\beta_i = \lg\left(\frac{A_k E_k}{RG(a)}\right) - 2.315 - 0.4567\frac{E_k}{RT_{pi}}$$

where $G(a)$ is the integral equation of the reaction. Activation energy E_k can be obtained from the slopes of the straight lines for the functions, with $\ln(\beta_i/T_{pi}^2)$ vs. $1/T_{pi}$ for the Kissinger method and $\lg\beta_i$ vs. $1/T_{pi}$ for the Ozawa method respectively.

Both Kissinger and Ozawa methods reveal a good linearity. The oxidation activation energy was caculated from the Kissinger and Ozawa curves. As shown in Table 2, the oxidation activation energies of graphite flake deduced from the Kissinger and Ozawa curves are 293.53 kJ/mol and 291.27 kJ/mol respectively, which are greater than 202.58 kJ/mol and 208.24 kJ/mol of EG. So, the oxidation activation energy results indicated that EG has higher reactivity than that of graphite flake.

4. Conclusions

The following conclusions were made on the basis of phase compositions, microstructures, and mechanical properties of Al_2O_3–C refractories fired from 800 to 1400 °C in coke bed.

(1) Graphene oxide nanosheets (GONs) were well distributed in α-Al_2O_3 powder by ball milling expanded graphite with micron sized α-Al_2O_3 powder, and the size and thickness of GONs depended on the addition amount of expanded graphite.
(2) GONs can accelerate the in-situ formation of ceramic whiskers in specimens because they have higher reactivity than graphite flake.
(3) GONs produced the strengthening effects on Al_2O_3–C refractories after firing at 800 °C and the synergetic strengthening effects with graphite flake and the in-situ formed whiskers after firing at 1000–1400 °C.

Acknowledgments

The authors thank the financial support from Natural Science Foundation of China (51002108) and Department of Science and Technology of China (2012CB722702), Wuhan Science and Technology Bureau (2013010602010210) and Natural Science Foundation of Hubei Province (2009CDA050).

References

[1] E. Mohamed, M. Ewais, Carbon based refractories, Journal of the Ceramic Society of Japan 112 (10) (2004) 517–532.
[2] B. Hashemi, Z.A. Nemati, M.A. Faghihi-Sani, Effects of resin and graphite content on density and oxidation behavior of MgO–C refractory bricks, Ceramics International 36 (2006) 313–319.
[3] M. Bavand-Vandchali, H. Sarpoolaky, F. Golestani-Fard, Atmosphere and carbon effects on microstructure and phase analysis of in situ spinel formation in MgO–C refractories matrix, Ceramics International 35 (2) (2009) 861–868.
[4] S. Zhang, W.E. Lee, Influence of additives on corrosion resistance and corroded microstructures of MgO-C refractories, Journal of the European Ceramic Society 21 (2001) 2393–2405.
[5] Leonardo Musante, Vanesa Munoz, Marcelo H. Labadie, Analía G. Tomba Martinez, High temperature mechanical behavior of Al_2O_3–MgO–C refractories for steelmaking use, Ceramics International 37 (2011) 1473–1483.
[6] Liu Bo, Sun Jialin, Tang Guangsheng, Liu Kaiqi, Li Lin, Liu Yongfeng, Effects of nanometer carbon black on performance of low-carbon MgO–C composites, Journal of Iron and Steel Research International 17 (10) (2010) 75–78.
[7] Li Lin, Tang Guang-sheng, He Zhi-yong, Influences of black carbon addition on mechanical performance of low-carbon MgO–C composite, Journal of Iron and Steel Research International 17 (12) (2010) 75–78.
[8] Y.W. Li, X.L. Chen, Y.B. Li, S.B. Sang, L. Zhao, Effect of multi-walled carbon nanotubes on the thermal conductivity and pore characteristic of blast furnace carbon refractories, Metallurgical and Materials Transactions A 41 (9) (2010) 2383–2388.

[9] Mousom Bag, Sukumar Adak, Ritwik Sarkar, Study on low carbon containing MgO–C refractory: use of nano carbon, Ceramics International 38 (3) (2012) 2339–2346.
[10] T. Matsui, T. Goto, Y. Yamada, N. Taki, Characteristics and application of nano-tech magnesia carbon bricks, UNITECR'05 Proceedings (2005) 627–631.
[11] S. Tamura, T. Ochiai, S. Takanaga, T. Kanai, H. Nakamura, Nakamura, Nano-tech refractories-1: the development of the nano structural matrix, UNITECR'03 Proceedings (2003) 517–520.
[12] Y. Morisada, Y. Miyamoto, Y. Takaura, K. Hirota, N. Tamari, Mechanical properties of SiC composites incorporating SiC-coated multi-walled carbon nanotubes, International Journal of Refractory Metals and Hard Materials 25 (2006) 322–327.
13 J. Wang, H.M. Kou, X.J. Liu, Y.B. Pan, J.K. Guo, Reinforcement of mullite matrix with multi-walled carbon nanotubes, Ceramics International 33 (2007) 719–722.
[14] Ming Luo, Yawei Li, Shengli Jin, Shaobai Sang, Lei Zhao, Yuanbing Li, Microstructures and mechanical properties of Al_2O_3–C refractories with addition of multi-walled carbon nanotubes, Materials Science and Engineering: A 548 (2012) 134–141.
[15] V. Roungos, C.G. Aneziris, Improved thermal shock performance of Al_2O_3–C refractories due to nanoscaled additives, Ceramics International 2 (38) (2012) 919–927.
[16] Steffen Dudczig, Dániel Veres, Christos G. Aneziris, Erik Skiera, Rolf W. Steinbrech, Nano- and micrometre additions of SiO_2, ZrO_2 and TiO_2 in fine grained alumina refractory ceramics for improved thermal shock performance, Ceramics International 3 (38) (2012) 1019–2011.
[17] C.G. Aneziris, J. Hubalkova, R. Bárábas, Microstructure evaluation of MgO-C refractories with TiO_2- and Al-additions, Journal of the European Ceramic Society 27 (2007) 73–78.
[18] A.S. Gokce, C. Guran, S. Ozgen, The effect of antioxidants on the oxidation behaviour of magnesia-carbon refractory bricks, Ceramics International 34 (2008) 323–330.
[19] Y.W. Li, C.G. Aneziris, X.X. Yi, S.L. Jin, N. Li, Formation of dumbbell-shaped β-SiC whiskers in advanced refractories for Al_2O_3–ZrO_2–C slide gate, Interceramics (2005) 20–23.
[20] Péter Kun, Orsolya Tapasztó, Férenc Wéber, Csaba Balázsi, Determination of structural and mechanical properties of multilayer graphene added silicon nitride-based composites, Ceramics International 38 (2012) 211–216.
[21] Young S.o.o. Yun, Yo Han Bae, Do Hyeong Kim, Reinforcing effects of adding alkylated graphene oxide to polypropylene, Carbon 49 (2011) 3553–3559.
[22] T. Ramanathan, A.A. Abdala, S. Stankovich, D.A. Dikin, M. Herrera-Alonso, R.D. Piner, D.H. Adamson, H.C. Schniepp, X. Chen, R.S. Ruoff, S.T. Nguyen, I.A. Aksay, R.K. Prud'Homme, L.C. Brinson, Functionalized graphene sheets for polymer nanocomposites, Nature nanotechnology 3 (2008) 327–331.
[23] K. Wang, Y.F. Wang, et al., Preparation of graphene nanosheet/alumina composites by spark plasma sintering, Materials Research Bulletin 46 (2011) 315–318.
[24] H.B. Fan, Y.W. Li, S.B. Sang, Microstructures and mechanical properties of Al_2O_3–C refractories with silicon additive using different carbon sources, Materials Science and Engineering: A 528 (2011) 3177–3185.
[25] Ji-hui Li, Li-li Feng, Zhi-xin Jia, Preparation of expanded graphite with 160 μm mesh of fine flake graphite, Materials Letters 60 (2006) 746–749.
[26] G.u.o. Chun-yu, W.a.n.g. Cheng-yang, Study on preparation of activated mesocarbon microbeads/expanded graphite composites for electrical double layer capacitors, Composites Science and Technology 67 (2007) 1747–1750.
[27] Y.C. Fan, L.J. Wang, J.L. Li, J.Q. Li, S.K. Sun, F. Chen, L.d. Chen, W. Jiang, Preparation and electrical properties of graphene nanosheet/Al_2O_3 composites, Carbon 48 (2010) 1743–1749.
[28] X.L. Chen, Y.B. Li, Y.W. Li, Carbothermic reduction synthesis of Ti(C, N) powder in the presence of molten salt, Ceramics International 34 (2008) 1253–1259.
[29] X.L. Chen, Y.W. Li, Y.B. Li, Effect of temperature on the properties and microstructures of carbon refractories for blast furnace (BF), Metallurgical and Materials Transactions A 40 (2009) 1675–1683.
[30] W.Z. Hu, S.L. Gao, F.Q. Zhao, Kinetics of thermal analysis, Science Press, Beijing, 2008.
[31] M.J. Starink, A new method for the derivation of activation energies from experiments performed at constant heating rate, Thermochimica Acta 288 (1996) 97–104.